SIRIOL

Gunn, M.; Duller, G.A.T.; Roberts, H.M.

Published in:
Radiation Measurements

DOI:
10.1016/j.radmeas.2022.106782

Publication date:
2022

Citation for published version (APA):
Gunn, M., Duller, G. A. T., & Roberts, H. M. (2022). SIRIOL: A Sensitive InfraRed Instrument for phOto Luminescence measurements of feldspar. *Radiation Measurements*, *154*, 106782. [106782]. https://doi.org/10.1016/j.radmeas.2022.106782

Radiation Measurements 154 (2022) 106782

Contents lists available at ScienceDirect

Radiation Measurements

journal homepage: www.elsevier.com/locate/radmeas

SIRIOL: A Sensitive InfraRed Instrument for phOto Luminescence measurements of feldspar

M. Gunn [a,*], G.A.T. Duller [b], H.M. Roberts [b]

[a] Department of Physics, Aberystwyth University, Ceredigion, SY23 3BZ, United Kingdom
[b] Department of Geography and Earth Sciences, Aberystwyth University, Ceredigion, SY23 3DB, United Kingdom

ARTICLE INFO

Keywords:
Infrared photoluminescence IRPL
Instrument development
Signal optimisation
luminescence imaging
Luminescence dating

ABSTRACT

The new InfraRed PhotoLuminescence (IRPL) signal in feldspar offers a promising alternative to the well-established OSL method to recover the absorbed radiation dose for dating purposes. The non-destructive readout using Stokes shifted photoluminescence offers the opportunity to carry out repeat measurements to improve the signal to noise ratio, and the steady state signal enables straightforward spatially and spectrally resolved measurements. However, the exploitation of the IRPL signal has been hampered by a large background signal, making the IRPL emission that is of interest for measuring absorbed dose difficult to discriminate.

A new IRPL detection attachment for the Risø luminescence reader has been developed which enables measurement of the IRPL emission with a signal to background at least two orders of magnitude higher than reported previously. These improvements have been achieved through a combination of a bespoke optical design along with careful selection of filters and coatings. Key instrument design details are presented along with some preliminary results from slices of museum specimens of feldspar.

1. Introduction

Luminescence dating techniques make use of rocks and sediments as natural dosimeters to record the ionising radiation dose absorbed since the last bleaching event (Rhodes 2011). In combination with a knowledge of the radiation dose rate to which the sample has been subjected, the time elapsed since its last bleaching event can be calculated to establish the date of burial (Duller 2008). Luminescence dating finds widespread use in archaeology, geomorphology and Quaternary science as it enables the chronology of past events to be determined.

The exposure of crystalline minerals such as quartz and feldspar in the sample to ionising radiation excites electrons from the ground state to a higher energy state, after which most return to the ground state. However, a proportion of these electrons are caught in traps formed by defects in the crystal structure and can remain trapped for geological periods of time. When exposed to a suitable stimulus such as light or heat, the electrons are excited out of the traps, and in the case of feldspars electrons may travel through the band tail states and return to the ground state at a recombination centre resulting in the emission of a photon of light (Poolton et al., 1995). Optically Stimulated Luminescence (OSL) excites the electrons from the trap using light with a lower photon energy than that emitted as the electrons relax to the ground state – an anti-Stokes emission. OSL is therefore a destructive measurement as the traps are depleted by the measurement process and so the measurement can only be made once. This prevents repeat measurements or signal averaging to improve the signal to noise ratio and hence limits the precision of the measurements. OSL measurements of feldspars are also complicated by processes such as anomalous fading (Wintle 1973) and so additional stimulation steps are required as part of the measurement cycle (Thomsen et al., 2008).

Prasad et al. (2017) announced the discovery of a dose dependent photoluminescent signal from feldspar with emissions at 955 nm when stimulated with light at 885 nm and Kumar et al. (2018) announced the discovery of a second emission at 880 nm when stimulated with light at 830 nm. These InfraRed PhotoLuminescence (IRPL) emissions arise from excitation of charge to an excited state within the defect and subsequent relaxation back to the ground state of the trap accompanied by a Stokes shifted emission (Jain et al., 2020), a process that does not require recombination of the charge. Thus, the signal can be measured repeatedly, enabling improved signal to noise ratio, and offering a promising alternative to the well-established OSL methods of absorbed dose measurement (Kumar et al., 2021). However, the proximity of the

* Corresponding author.
E-mail address: mmg@aber.ac.uk (M. Gunn).

https://doi.org/10.1016/j.radmeas.2022.106782
Received 21 December 2021; Received in revised form 1 April 2022; Accepted 2 May 2022
Available online 10 May 2022

stimulation and emission wavelengths results in breakthrough of the stimulation light to the detector which limits the dynamic range of the measurements. For instance, Kook et al. (2018) reported breakthrough of 1×10^4 ct s^{-1} during stimulation with a 3 mW cm^{-2} laser (830 nm) when measuring the 880 nm emission using a photomultiplier. They were able to overcome this problem by using a pulsed stimulation source and time resolved measurements (Kook et al., 2018) but this method is unsuitable for spatially resolved measurements. Sellwood et al. (2019, 2022) have developed a stand-alone instrument for spatially resolved IRPL and IRSL measurements of rock samples which achieved a background of between 50 and 150 cts/pixel/s, depending on the reflectivity of the sample, which is about 10 times lower than Duller et al. (2020), but still significant. Additionally, the Sellwood et al. (2022) system requiremes the sample to be moved to another instrument for dosing and heating, preventing it being used for automated measurement sequences. Kook et al. (2018) and Thomsen et al. (2018) each present a single spatially resolved IRPL measurement of a granite sample taken with a Risø instrument, but it is hard to assess the background of this instrument. While TL, $IRSL_{50}$ and $pIRIR_{225}$ signals from the granite slice show a wide dynamic range and with some values close to zero, the IRPL signal has a dynamic range of less than 2 (ratio of the highest signal divided by the lowest signal) (Fig. 5a in Thomsen et al., 2018). In order to investigate the various luminescence signals from feldspar in more detail, a versatile instrument capable of making spatially resolved IRPL measurements with a low background was required. This paper describes the development and optimisation of a new optical head for measurement of the IRPL signal from feldspar, which can be integrated with the Risø luminescence reader, alongside the existing DASH head (Lapp et al., 2015). The improvement in signal-to-noise ratio compared with our previous IRPL system (Duller et al., 2020) is demonstrated using measurements of single grains of potassium-rich feldspar, and the versatility and sensitivity of the instrument are demonstrated through examination of emissions from slices of some museum specimens of feldspar.

2. Instrument development and optimisation

Initial attempts to measure IRPL at Aberystwyth were made by retrofitting a stimulation source comprised of an 850 nm laser with a narrow band pass clean-up filter and ground glass diffuser to the spare port on the Risø DASH head (Lapp et al., 2015). Detection of the IRPL signal was performed by the DASH head EMCCD with 925 nm long pass and two 950 nm (50 nm band pass) filters installed in the inbuilt filter wheels to allow the IRPL signal to be discriminated from the stimulation laser. With each detection filter specified to have a rejection ratio of at least 10^4 at the laser wavelength, a stack of 3 should have a rejection ratio of at least 10^{12}. With an IRPL signal of the order of 10^{-5} of the stimulation power, it should have been straightforward to discriminate the IRPL signal from the stimulation source. However, IRPL measurements from this setup showed a very small signal on top of a very large background, resulting in poor use of the detector's dynamic range and making effective discrimination of the IRPL signal almost impossible and so measurements with this setup were not pursued further.

The largest contribution to the background was caused by breakthrough of the thin film interference filters by stimulation light passing through at large angles as described previously in Duller et al. (2020). The approach taken by Duller et al. (2020) to overcome this issue was to remove the DASH head (with all its anodised surfaces) and design a bespoke attachment for imaging IRPL where the coatings were optimised, and the imaging lens system designed to reduce scatter. Further details of the implemented solution are given in sections 2.1 and 2.2 before going onto describe the new system.

2.1. Coatings

The inside of the DASH head and lens assembly is finished with black anodise to minimise scattering and stray light. Although this black anodise has a low reflectance in the visible spectral range, it is not optimal for the near InfraRed range where the IRPL stimulation and emission from feldspar occurs. The diffuse reflectance of black anodised components from the Risø instrument and anodised components from Thorlabs were measured with an Ocean Optics Flame spectrometer and ISP-REF integrating sphere probe and calibrated to a Labsphere Spectralon reflectance standard. It can be seen from these results (Fig. 1) that the reflectance of anodised surfaces rises rapidly from around 680 nm and that the surfaces of the DASH head have a diffuse reflectance of at least 35% at 830 nm, allowing multiple scattering events and enabling stray light to propagate through the system. Reflectance measurements were also made for an acrylic black paint ('Black 2.0'). In contrast to the anodised surfaces, the Black 2.0 paint has an almost constant reflectance of around 3% throughout the measured spectral range. Although more sophisticated black coatings are available, the availability and ease of application of Black 2.0 makes it ideal for prototype developments applications such as those described in this paper.

2.2. Optical system

A bespoke optical system was developed using commercial off the shelf (COTS) optical components. The imaging optics consist of Thorlabs IR anti-reflection coated 100 mm and 80 mm achromatic doublets in a semi symmetric lens design which provides reasonable control of aberrations over the required field of view. The filters are located between the focussing elements where the rays are collimated, and the angle of incidence is minimised. A baffle near the sample reduces the amount and angle of stray light reaching the lenses and the inside of all optical tubes and mounts are coated with Black 2.0 to minimise reflectance in the infrared.

Using the optimised coatings and lens system the IRPL head described by Duller et al. (2020) was able to successfully image IRPL from single feldspar grains mounted in a 10 by 10 grid on an aluminium disc. Although the system was able to generate useful data, capable of investigating the resetting of the IRPL signal, and use it for dating of single grains, the signal-to-background ratio was poor (0.59; Duller et al., 2020). The system also had several limitations. Firstly, since an 850 nm laser diode was used for stimulation, it was only possible to detect the 955 nm IRPL emission, not the 880 nm emission. Secondly, the IRPL head replaced the DASH head on the Risø reader and thus it was not possible to measure other luminescence signals such as TL or IRSL, and the ability to change detectors and detection filters that the DASH provides was also lost. The design of the new imaging IRPL unit described in section 3 aimed to overcome these limitations, and to reduce the breakthrough still further thus improving the signal-to-background ratio significantly.

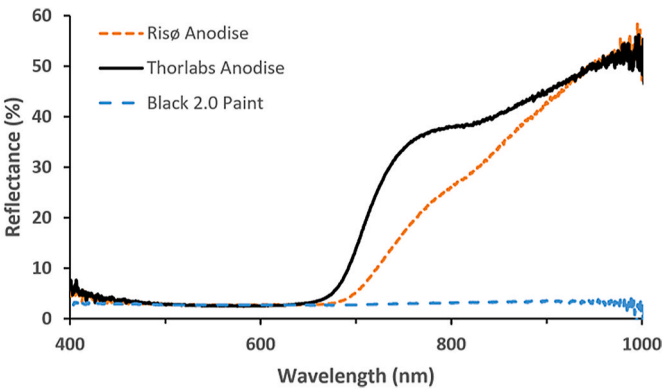

Fig. 1. Diffuse reflectance measurements of black finishes.

3. Instrument description

The Sensitive InfraRed Instrument for phOto Luminescence (SIRIOL) described here is a new optical head that builds on the experience gained from the previous system (Duller et al., 2020). The system retains the vertical imaging optics from the earlier system, but it has four key differences. Firstly, SIRIOL is not mounted over the hotplate, but instead it is located on the lid of the Risø reader where there is an aperture in the location on the Risø reader sometimes used for an alpha irradiator, giving access to samples mounted on the carousel. This allows the DASH head to be used for the purpose for which it was optimised, providing blue, green and infrared optical stimulation, an automated filter changer, and a detector changer equipped with two photomultipliers (EMD-9107 and H7421-40) and a Photometrics Evolve 512 Electron Multiplying Charge Coupled Device camera to permit imaging of TL, OSL and IRSL. Secondly, as well as keeping the DASH head equipped with its EMCCD, a second Photometrics Evolve 512 EMCCD is used for SIRIOL, making it possible to image IRPL in the same sequence of measurements as TL, IRSL and OSL are imaged with the DASH head. Thirdly, an 830 nm laser diode and controller from ThorLabs equipped with a 830 nm (10 nm bandpass) filter is used for stimulation of IRPL (Kumar et al., 2018; Kook et al., 2018) instead of the 850 nm one used previously (Duller et al., 2020), opening up the possibility of detecting the 880 nm IRPL emission (Kumar et al., 2018), and increasing the spectral distance between stimulation and detection to help reduce breakthrough. A ground glass diffuser is used to ensure the sample is uniformly illuminated with a power density of 10 mW cm^{-2} – half that used previously. Fourthly, a Thorlabs motorised filter changer has been inserted between the two lenses to enable automated selection of different spectral emission regions. In addition, one space in the filter wheel is occupied by a 5 mm diameter aperture to improve the resolution for reflected light imaging. A proprietary ~900 nm long pass filter with a very high rejection ratio (>10^8) is permanently mounted in the imaging optics assembly which provides much greater suppression of the stimulation laser light. The rejection ratio of the different filter combinations was measured by directing the 830 nm laser with clean-up filter at a silicon photodiode connected to a calibrated Thorlabs photodiode current amplifier with digital readout. By using the full dynamic range of the photodiode current amplifier and a set of calibrated neutral density filters it was possible to measure rejection ratios as high as 10^{10}. The spectral transmission of the combined filters is shown in Fig. 2 along with an IRPL emission spectrum reproduced from Kumar et al. (2018), and technical details are presented in Table 1. The long pass filter cuts off the short wavelength end of the BP900 filter pass band and prevents the detection of light below ~890 nm. Although the system is not able to measure the peak of the IRPL 880 nm emission, the tail of this emission is detected as it is quite broad, even at low temperature as shown in Fig. 2 and Kumar et al. (2018).

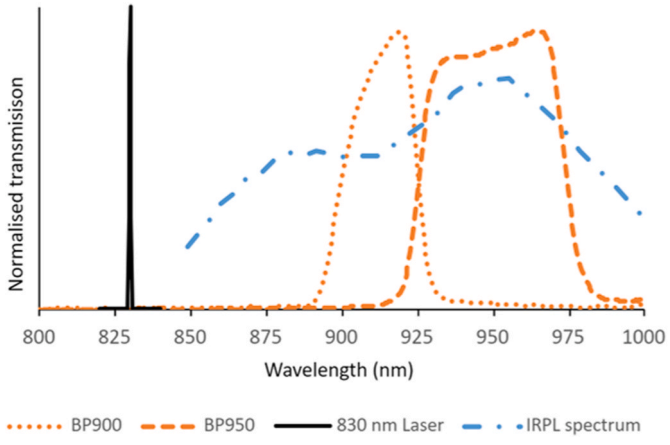

Fig. 2. Stimulation and detection bands for SIRIOL. The IRPL emission spectrum is reproduced from Kumar et al. (2018) Fig. 4b and was measured at 7K - at room temperature the two emission peaks will be even broader.

Table 1
Summary of the main optical components in SIRIOL.

Stimulation sources	Wavelength	Bandwidth (FWHM)	Power Density at sample
Stimulation laser diode with clean-up filter	830 nm	Laser line width ~0.5 nm 10 nm clean-up filter	10 mW/cm^2
Reflected light imaging LED	880 nm	50 nm	150 μW/cm^2
UV Bleaching LED	375 nm	9 nm	400 mW/cm^2
Detection			
Detector	Photometrics Evolve 512 EMCCD camera		
Imaging Lenses	Thorlabs 100 mm and 80 mm IR achromatic doublets		
Detection filters [& location]	Centre wavelength/50% Cut off	Bandwidth	Rejection ratio
Long pass (Proprietary) [fixed]	900 nm	–	1.5 × 10^9
900 Band Pass (Edmund optics) [filter wheel]	900 nm	50 nm	~10^4 (not measured)
950 Band Pass (Edmund Optics) [filter wheel]	950 nm	50 nm	1.5 × 10^6

The SIRIOL head includes three ports at a 30° angle of incidence, one for the 830 nm laser used to stimulate IRPL, one for a 375 nm high-power LED for bleaching the sample and one for an 880 nm LED which overlaps with the detection passband and is used for imaging the sample under reflected rather than emitted light. A diagram and photo of the new IRPL optical head is shown in Fig. 3.

The IRPL optical head light source control electronics are interfaced to spare I/O ports on the Risø reader, enabling the IRPL measurements to be automated via the Risø Sequence Editor software. The combined instrument includes both the DASH and IRPL measurement heads, enabling fully automated measurement sequences involving any combination of: beta irradiation, heating, OSL and IRSL using a photomultiplier, imaging OSL, imaging IRSL, imaging thermoluminescence, imaging IRPL and UV bleaching for a single or multiple samples. This versatility enables direct comparison of multiple dose dependent luminescence signals from samples, allowing the relationship between these different signals to be explored.

3.1. Instrument fluorescence

Testing of SIRIOL indicated that the background during IRPL measurements was lower than that reported previously (Duller et al., 2020), but that the background was dependent on the nature of the sample holder: anodised aluminium discs such as standard Risø single grain discs yielded a high background and steel discs gave a much lower background (Table 2). From this it was deduced that the aluminium oxide was fluorescing in the same detection wavelength range as the feldspar IRPL emission. This observation of fluorescence also explains why the instrument described by Duller et al. (2020) had a lower background than we saw (unpublished data) when using the approach of Kook et al. (2018) of using a modified DASH head for IRPL measurements – all of the internal surfaces of the DASH head are anodised and so will have been fluorescing in addition to being highly reflective.

All anodised surfaces inside the Risø reader which were within or near the field of view of SIRIOL and which could give rise to fluorescence, such as the internal surfaces of the Risø reader under the sample carousel were coated with Black 2.0 or covered with Thorlabs black aluminium foil. A sample carousel which had previously been painted by

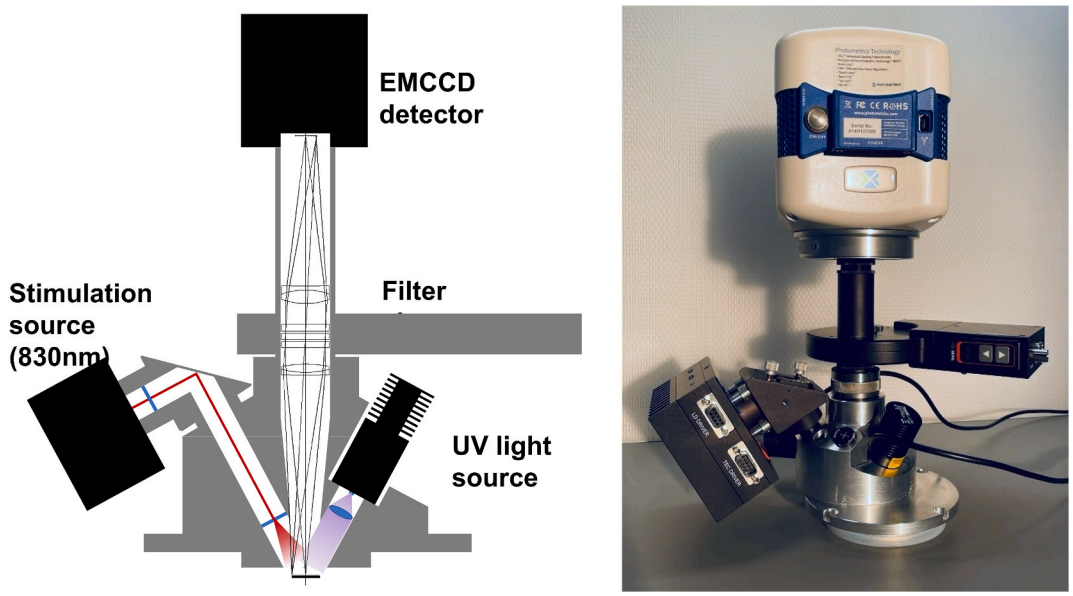

Fig. 3. Left: Cross section diagram and Right: photograph of SIRIOL.

Table 2
IRPL signals detected through BP900 and BP950 filters from empty sample carriers made of different metals, and with different coatings.

Material	Coating	BP900 (cts/pixel/s)	BP950 (cts/pixel/s)
Aluminium single grain disc	Anodised	2.33	3.10
Aluminium single grain disc	None	0.41	0.38
Aluminium single grain disc	Gold sputtered	0.48	0.39
Aluminium flat disc	None	0.30	0.25
Aluminium flat disc	Gold sputtered	0.57	0.44
Copper	Rhodium plated	0.07	0.01
Stainless Steel single grain disc	None	0.07	0.05

the manufacturers with IR absorbing paint was used exclusively for subsequent measurements. Steel cups were subsequently used for all measurements of bulk samples and for single grain measurements stainless-steel single grain discs were manufactured in-house using laser machining.

The IRPL signal to background ratio of SIRIOL with the stainless-steel single grain discs was determined from measurement of a disc containing single grains of potassium-rich feldspar separated from sample GDNZ45 (Duller 1996). A dose of ~20 Gy was given to the disc, preheated at 250 °C for 60 s, the IRSL measured for 100 s, and then the IRPL measured for 6 s. A transect was taken across a line of single grains and the intensity of the luminescent signal plotted to show the signal in comparison to the background from the disc. Fig. 4 compares the results published from a previous version of this instrument described in Duller et al. (2020) with those from this instrument when using the new sample discs. The reduction in absolute signal (cts/s/pixel) from the feldspar grains using SIRIOL compared to the previous instrument is due to a combination of the reduced background, changing the stimulation laser wavelength from 850 to 830 nm, the fact that the laser power has been halved, and an increase in the attenuation in the imaging optics due to the additional long pass filter. Nevertheless, as can be seen from Fig. 4 the ratio of signal to background for SIRIOL is at least two orders of magnitude greater than the previous system and is now around 50 for this sample at this dose (~20 Gy).

3.2. Reproducibility of 830 nm stimulation

The IRPL signal varies linearly with the power of the infrared stimulation source, and so it is important to assess its stability and reproducibility. The temperature of the 830 nm laser diode used on SIRIOL is thermoelectrically controlled, and the laser diode is operated in constant power mode with feedback provided by the integrated photodiode. The stability of the laser output has been measured using a Thorlabs laser power meter with an integrating sphere detector. When switched on the laser power can fluctuate by a few percent over the first second or so. The laser is therefore switched on and allowed to stabilise for at least 2 s before the measurement sequence is begun. Over a typical measurement sequence of around 20 s, the power was found to fluctuate by less than 0.3%. Analysis of repeated measurements during a sequence lasting 5 days showed excellent reproducibility, with an average relative standard deviation of 0.6%. This reproducibility is also corroborated by pulse annealing data (e.g. Fig. 7b) presented in the next section.

4. Application to pulse annealing

To demonstrate the potential of the combination of the DASH head and SIRIOL, measurements were made of multiple luminescence emissions from three museum specimens of feldspar. Each sample was sliced with a diamond wafer blade to produce slices ~200 μm thick and approximately 5 x 5 mm. These slices were placed on steel cups for analysis. The feldspars are orthoclase (McDonald Ranges, Northern Territories), microcline (Arkaroola, #7) and oligoclase (unknown location, #19) and have previously been chemically characterised by Prescott and Fox (1993) who also measured their TL emission spectra.

A pulse annealing experiment was undertaken to assess the thermal dependence of a range of luminescence signals from the three samples. The DASH head was used for measurements of TL, IRSL while holding at 50 °C ($IRSL_{50}$) and a subsequent post-IR IRSL measurement while holding the sample at 225 °C ($pIR\text{-}IRSL_{225}$). The blue emission was isolated for the TL, IRSL and pIR-IRSL measurements using a combination of Schott BG3 and Schott BG39 glass. IRPL measurements were undertaken using SIRIOL, and two sets of filters were used to isolate the 880 nm IRPL signal (BP900Δ50 nm) and the 955 nm IRPL emission (BP950Δ50 nm). The procedure followed is given in Table 3. Prior to starting this sequence, the slices underwent 10 cycles of irradiation and heating to 500 °C to reduce the magnitude of sensitivity change during this pulse annealing experiment. The lack of sensitivity change caused by these treatments was confirmed by remeasuring data for temperatures in Step 2 of 100, 200, 300, 400 and 500 °C at the end of the pulse

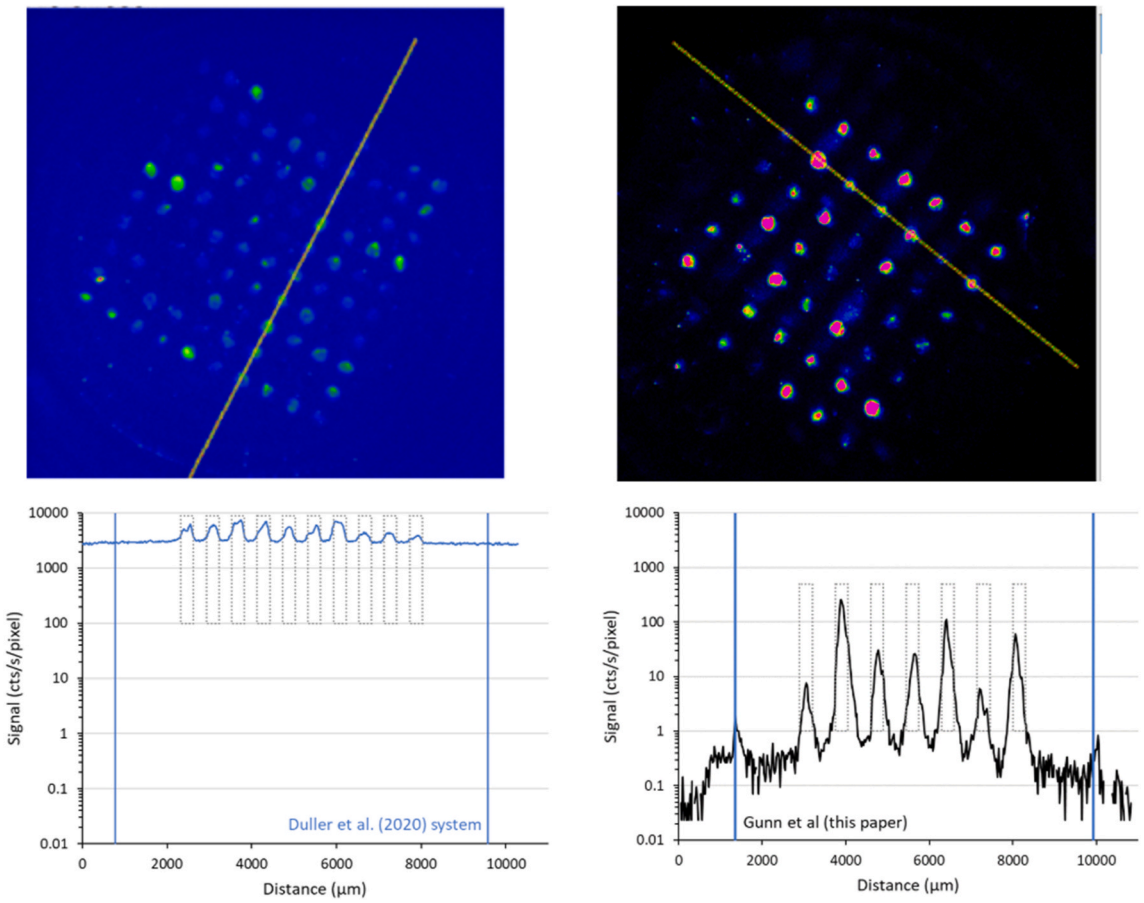

Fig. 4. Transects through single grain discs showing the IRPL signal to background ratio for: Left – sample GDNZ16 (dose ~100 Gy) in anodised Aluminium 10 by 10 single grain disc measured with the instrument described in Duller et al. (2020), Right – sample GDNZ45 (dose ~ 20 Gy) in stainless steel 7 by 7 single grain disc measured with SIRIOL.

annealing sequence, and all repeat measurements were within 10%. A final set of measurements from steps 1 to 13 were undertaken with pulse annealing at 500 °C, but with the TL signal in Step 2 measured with a combination of a Schott OG550 and a Schott BG39 (572 nm FWHM 66 nm) to isolate the yellow (~570 nm) emission; these measurements could then be used to assess the relative emissions of the three samples in the yellow and blue.

Fig. 5 shows TL data for the three samples. This microcline has a narrow TL peak at ~150 °C, with minor high temperature peaks at ~330 and 440 °C (Fig. 5a, d). The orthoclase is similar except the low temperature peak extends from ~80 to 150 °C (Fig. 5c, d). As previously observed by Prescott and Fox (1993) and Duller (1995), this oligoclase has a very broad TL peak extending from below 100 °C to above 300 °C (Fig. 5b and d). For each mineral, there is little difference between the shape of the TL curves observed in the blue or yellow (Fig. 5d). Riedesel et al. (2021a) observed very intense yellow emission from single-phase K-rich and Na-rich feldspars and suggested that the ratio of blue to yellow emissions may be a useful diagnostic tool to differentiate between perthitic and single-phase feldspars; they also observed lower anomalous fading rates in single phase samples. The relative intensity of the blue and yellow emissions varies substantially for these three samples. Summing the signal from 100 to 200 °C, the ratio of the blue to yellow emission is 10.9 and 11.0 for the Microcline and Orthoclase, but only 1.5 for the Oligoclase, consistent with the bright emission in the yellow seen by Prescott and Fox (1993).

Fig. 6 shows the spatial distribution of $IRSL_{50}$, pIR-$IRSL_{225}$, and the two IRPL emissions for the microcline sample. The two infrared stimulated luminescence signals (Fig. 6a and b) show peak intensities in similar parts of the sample. These correspond to the white, milky looking areas seen in the visible photograph of the sample (Fig. 6e), while the darker areas on the photograph tend to have lower intensity IRSL signals (blue colours in Fig. 6a and b). The two IRPL emissions have very similar patterns of intensity as each other (Fig. 6c and d), but there are some notable differences with the IRSL data. In particular the area in the top left of the slice has very little IRSL, but some of the brightest IRPL signals (red colours in Fig. 6c and d). This top left corner has a very obvious fracture in the visible photograph, and the intense IRPL seems linked to this feature. Further analysis is required to explore the relationships between the different signals shown in Figs. 6 and 5a.

Fig. 6f shows the change in 5 different luminescence signals from the microcline as a function of the annealing temperature. For this analysis, the signal from the whole sample was summed. The $IRSL_{50}$ and pIR-$IRSL_{225}$ signals are calculated as the sum of the first second of IRSL signal, with a background from the last 5 s of measurement subtracted. The $IRSL_{50}$ signal remains relatively constant until a temperature of 160 °C, but when heated above this temperature the $IRSL_{50}$ signal drops rapidly, reaching near zero at 380 °C. In contrast the pIR-$IRSL_{225}$ drops monotonically as the annealing temperature is increased, but at a slower rate, so that it is not until a temperature of 540 °C that the signal is close to background. The two IRPL signals were calculated as the sum of the signal over 20 s of measurement (steps 5 or 6 in Table 3) minus the background signal (measured in steps 11 or 12). This background signal is what remains after resetting the signal using a combination of IR stimulation at 225 °C (step 7), exposure to UV for 600 s (step 8) and measuring the TL to 500 °C (step 9). The IRPL images measured in steps 11 and 12 show very similar patterns of bright and dim areas ('structure') as seen in steps 5 and 6 (Fig. 6c and d). For this microcline, the background makes up 88% of the $IRPL_{880}$ signal at low annealing

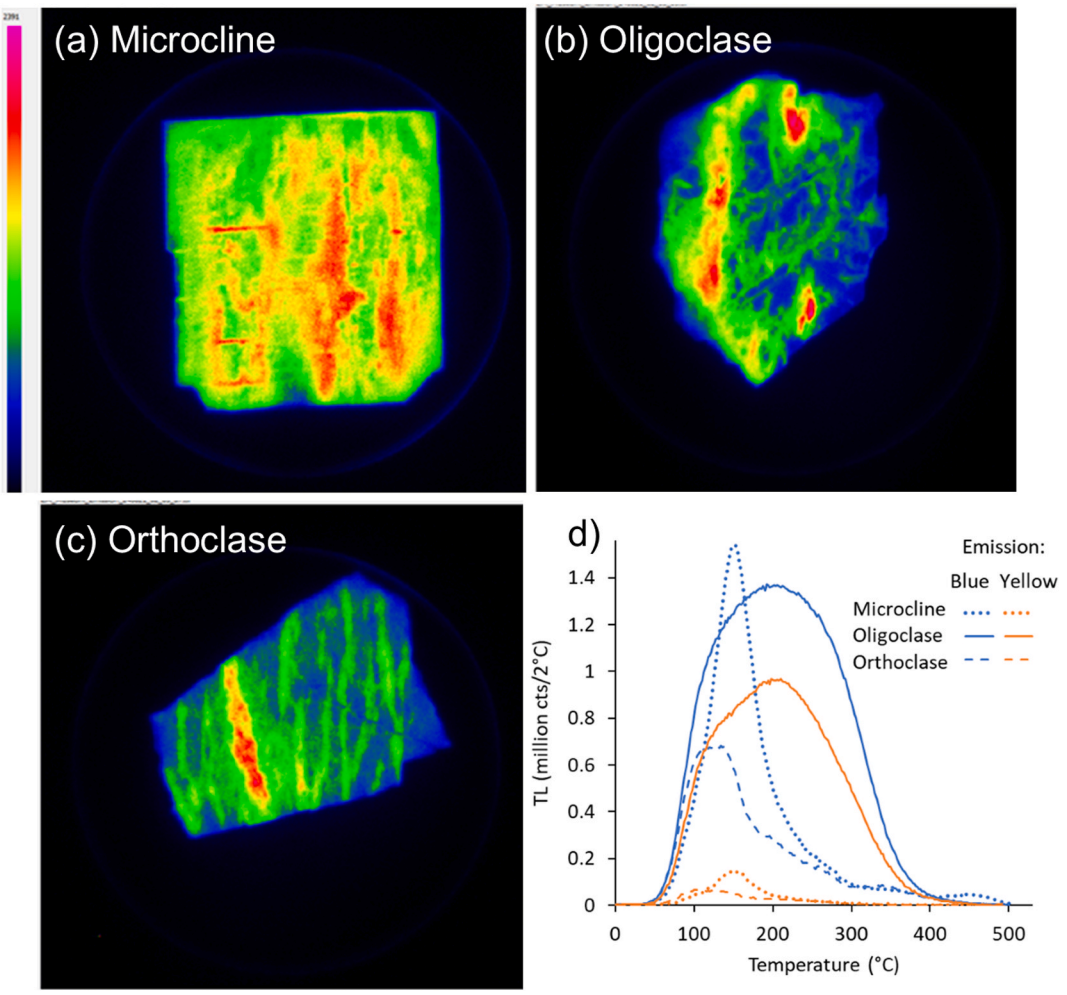

Fig. 5. Images of the 100–200 °C TL data (blue emission) for (a) Microcline, (b) Oligoclase and (c) Orthoclase. (d) TL data for all 3 samples heated to 500 °C at 5 °C. s^{-1}. For each sample the blue line shows emission at ~400 nm (FWHM 108 nm), and the orange line shows emission at ~570 nm (FWHM 66 nm). For the images in (a–c) the colours show intensity of the emission going from low intensity (black) to high intensity (red).

Table 3
Pulse annealing procedure. This was repeated for temperatures in Step 2 from 60 to 540 °C in 20 °C increments.

Step	Treatment	System
1	Irradiation ~100 Gy	–
2	TL at 5 °C.s^{-1} to temperature T°C (60, 80,100 … 540 °C)	DASH
3	Pause x seconds	–
4	$IRSL_{50}$ for 50 s	DASH
5	$IRPL_{880}$ for 20 s	SIRIOL
6	$IRPL_{955}$ for 20 s	SIRIOL
7	$IRSL_{225}$ for 100 s	DASH
8	UV bleaching for 600 s	SIRIOL
9	TL at 5 °C.s^{-1} to 500 °C	DASH
10	$IRSL_{50}$ for 50 s	DASH
11	$IRPL_{880}$ for 20 s	SIRIOL
12	$IRPL_{955}$ for 20 s	SIRIOL
13	$IRSL_{225}$ for 100 s	DASH

temperatures (60–120 °C), while for the $IRPL_{955}$ signal the value is 80% (shown in Fig. 7a), consistent with previous observations that the 955 nm emission is more susceptible to bleaching than the 880 nm emission (Kumar et al., 2021). As previously observed by Jain et al. (2020) the two signals show no loss as a result of annealing between 60 and ~360 °C, with the trend being for an increase by ~15%. Above 380 °C both IRPL signals drop, with the $IRPL_{955}$ emission dropping slightly faster, though the difference is small.

Resetting the IRPL signal either thermally (Fig. 6f) or optically (Kumar et al., 2020, 2021; Duller et al., 2020) is difficult. Duller et al. (2020) measured the reduction of the IRPL signal by exposure to different light sources. However, after long exposures to these light sources it was challenging to distinguish between the low IRPL signal remaining and the large instrumental background originating from breakthrough of the stimulation light or fluorescence of surfaces within the reader. The new IRPL system used here has a much lower background. Measurements on a blank steel cup (Fig. 7d) demonstrate that the background on SIRIOL is ~0.08 cts/pixel/s for the $IRPL_{955}$ signal (similar to that observed in Fig. 6 for a steel single grain disc, ~0.1–0.3 cts/pixel/s). Fig. 7a is derived from the same $IRPL_{955}$ data shown in Fig. 6f. The $IRPL_{955}$ data for the microcline slice in Fig. 7a is expressed as counts per pixel per second, and has not had any background subtracted. Data for IRPL in Fig. 6f was obtained by taking the measurement from step 6 of Table 3 and subtracting the signal in step 12, whereas these two signals are shown separately in Fig. 7a (blue data points are the signal and orange data points are the 'background' signal). Even after bleaching with infrared for 100 s while holding the sample at 225 °C (step 7), bleaching with the 375 nm UV LED for 600 s (step 8), and heating the sample to 500 °C (step 9), the microcline still gives an $IRPL_{955}$ signal of ~43 cts/pixel/s, compared with a signal of ~55 cts/pixel/s prior to bleaching. At annealing temperatures above ~380 °C the IRPL signal from the microcline does drop, but ~80% of the IRPL signal remains unaffected by steps 7 to 9 designed to remove the

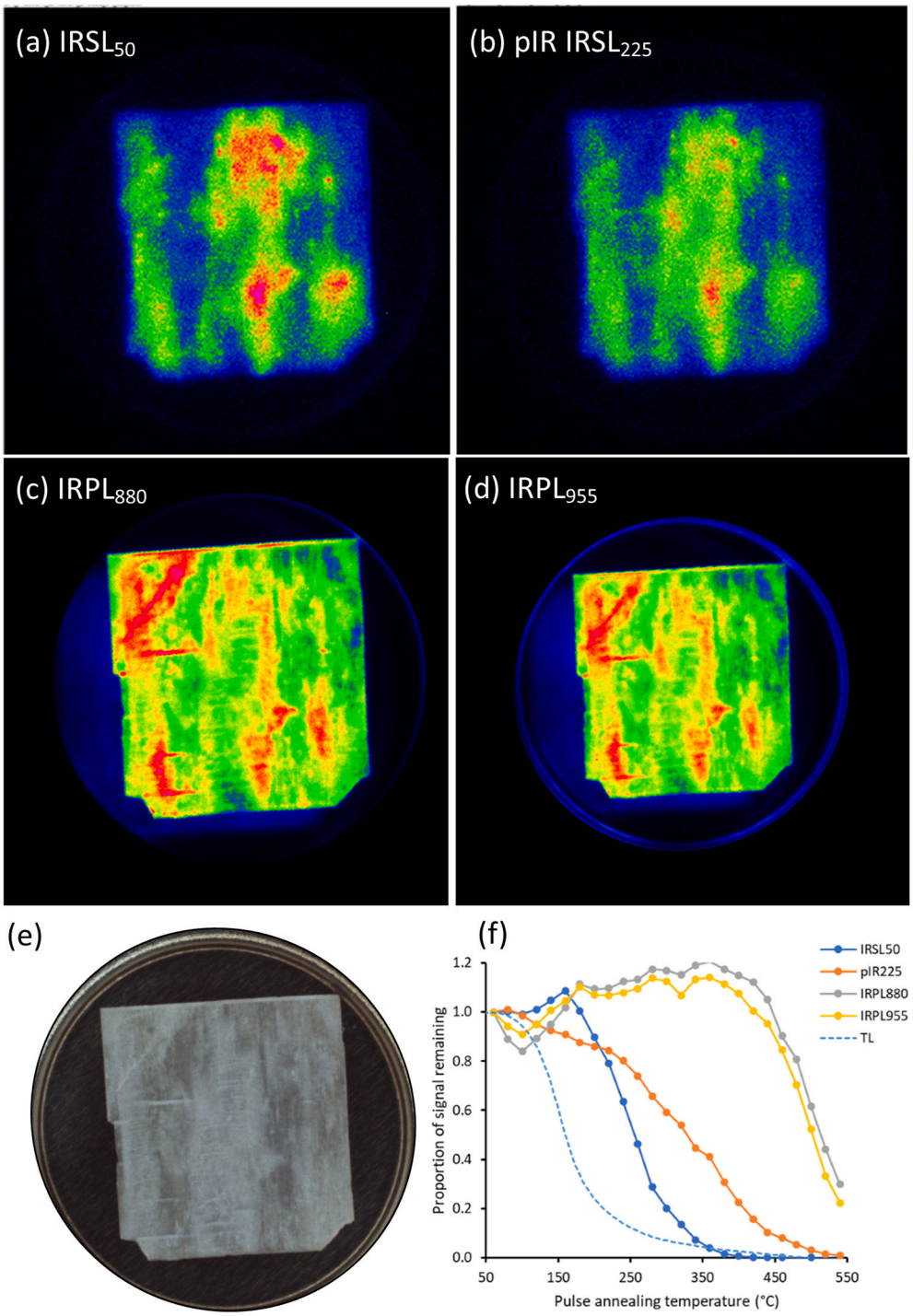

Fig. 6. Different luminescence signals from the microcline slice, along with a visible image (e) and (f) data for the pulse annealing experiment for these signals, all normalised to the first data point. For the images in (a) to (d) the colours show intensity of the emission going from low intensity (black) to high intensity (red).

signal. The sample was placed in a SOL2 solar simulator for 6 days and then had its IRPL remeasured, and this prolonged exposure to a broad spectrum did reduce the IRPL to ~19 cts/pixel/s.

Riedesel et al. (2021b) noted that the extent to which exposure to 18 h of SOL2 reset the IRPL emissions varied for their different feldspars, and this is also seen here (Fig. 7). Of the three feldspars, the orthoclase (Fig. 7c) is most effectively reset, but even for this sample the long SOL2 exposure is able to reduce the signal below the level achieved by the elevated temperature IR exposure, UV LED, and heating to 500 °C. The oligoclase has an extremely intense $IRPL_{955}$ emission, but it does not appear to be affected by pulse annealing to 540 °C (Fig. 7b). A substantial signal remains even after 6 days in the SOL2 (~60 cts/pixel/s, equivalent to ~8 million counts per second in the ~141 thousand pixels making up the region of interest), and hence it is unclear how useful this type of feldspar would be for dating. Variation in feldspar mineralogy, either between different crystals in rock samples or between different grains separated from geological sediments will occur, and the results presented here imply that spatially resolved measurements or single grain measurements may be needed to cope with the variability in the bleaching characteristics of the IRPL signal.

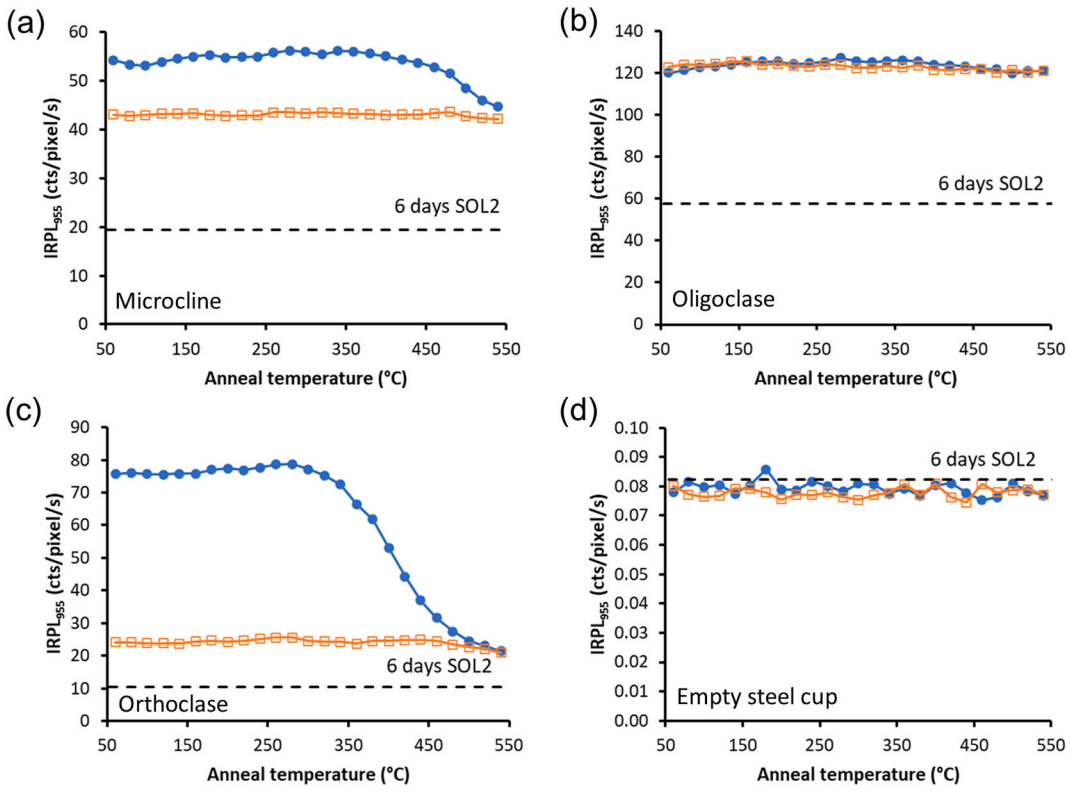

Fig. 7. $IRPL_{955}$ data for the three feldspars (a) Microcline, (b) Oligoclase, (c) Orthoclase and (d) an empty steel cup. Filled blue circles are the IRPL signal after heating to the specified temperature, and open orange squares are the signal remaining after measuring the IRSL signal while holding at 225 °C for 100 s, bleaching with the UV LED for 600 s and heating to 500 °C (referred to as the 'background' signal in the main text).The horizontal dashed black line shows the signal intensity measured after samples were put in the SOL2 solar simulator for 6 days.

5. Conclusions

A new Sensitive InfraRed Instrument for phOtoLuminescence (SIRIOL) has been developed for measurement of IRPL from feldspar. SIRIOL has been optimised to reduce the background signal and provides significantly greater discrimination of the spatially resolved IRPL signal from feldspar than has been achieved previously. SIRIOL has been integrated with the Risø reader, enabling automated sequences of imaging luminescence measurements to be made using both SIRIOL and the Risø DASH heads on the same sample.

The signal to background ratio has been improved by two orders of magnitude compared with the previous system (Duller et al., 2020) and has been achieved through a combination of bespoke imaging optics, improved stray light control, stimulation laser optimisation, a proprietary long pass filter, and the elimination of fluorescent surfaces within the instrument. The instrument background for the system described by Duller et al. (2020) was ~1000 cts/pixel/s, that for the system described by Sellwood et al. (2022) is between 50 and 150 cts/pixel/s, while SIRIOL is ~0.08 cts/pixel/s (Fig. 7d). The reduction in background of SIRIOL compared to our previous IRPL instrument has been measured using single grain discs of well characterised potassium-rich feldspar.

The combined use of SIRIOL and the Risø DASH head has been tested on slices cut from three museum specimens of feldspar measured through a pulse annealing sequence. This has enabled a direct comparison within an automated sequence of the TL, IRSL and IRPL signals from the same samples. The very low background of SIRIOL has allowed the resetting of the IRPL signal from different feldspar minerals to be investigated in greater detail than has previously been possible. It was found that of the samples tested, orthoclase is most readily reset and that oligoclase does not readily reset which has implications for its use in dating applications.

Declaration of competing interest

The authors declare that they have no known competing financial interests or personal relationships that could have appeared to influence the work reported in this paper.

Acknowledgements

This work was supported by the UK Space Agency (grant ST/P001998/1) and also forms part of the HEFCW supported SPARCL initiative at the Aberystwyth Luminescence Research Laboratory (ALRL) in Aberystwyth University. We thank the reviewers for their helpful comments which have greatly improved the manuscript.

References

Duller, G.A.T., 1995. Infrared bleaching of the thermoluminescence of four feldspars. J. Phys. Appl. Phys. 28, 1244–1258.
Duller, G.A.T., 1996. The age of the Koputaroa dunes, southwest North Island, New Zealand. Palaeogeogr. Palaeoclimatol. Palaeoecol. 121, 105–114.
Duller, G.A.T., 2008. Luminescence Dating: Guidelines on Using Luminescence Dating in Archaeology. English Heritage.
Duller, G.A.T., Gunn, M., Roberts, H.M., 2020. Single grain infrared photoluminescence (IRPL) measurements of feldspars for dating. Radiat. Meas. 133, 106313.
Jain, M., Kumar, R., Kook, M., 2020. A novel coupled RPL/OSL system to understand the dynamics of the metastable states. Sci. Rep. 10 (1), 15565.
Kook, M., Kumar, R., Murray, A.S., Thomsen, K.J., Jain, M., 2018. Instrumentation for the non-destructive optical measurement of trapped electrons in feldspar. Radiat. Meas. 120, 247–252.
Kumar, R., Kook, M., Murray, A.S., Jain, M., 2018. Towards direct measurement of electrons in metastable states in K-feldspar: do infrared-photoluminescence and radioluminescence probe the same trap? Radiat. Meas. 120, 7–13.
Kumar, R., Kook, M., Jain, M., 2020. Understanding the metastable states in K-Na aluminosilicates using novel site-selective excitation-emission spectroscopy. J. Phys. Appl. Phys. 53, 465301.
Kumar, R., Kook, M., Jain, M., 2021. Sediment dating using infrared photoluminescence. Quat. Geochronol. 62, 101147.

Lapp, T., Kook, M., Murray, A.S., Thomsen, K.J., Buylaert, J.P., Jain, M., 2015. A new luminescence detection and stimulation head for the Risø TL/OSL reader. Radiat. Meas. 81, 178–184.
Poolton, N.R.J., Bøtter-Jensen, L., Johnsen, O., 1995. Thermo-optical properties of optically stimulated luminescence in feldspars. Radiat. Meas. 24, 531–534.
Prasad, A.K., Poolton, N.R., Kook, M., Jain, M., 2017. Optical dating in a new light: a direct, non-destructive probe of trapped electrons. Sci. Rep. 7 (1), 12097.
Prescott, J.R., Fox, P.J., 1993. Three-dimensional thermoluminescence spectra of feldspars. J. Phys. Appl. Phys. 26, 2245–2254.
Rhodes, E.J., 2011. Optically stimulated luminescence dating of sediments over the past 200,000 years. Annu. Rev. Earth Planet Sci. 39, 461–488.
Riedesel, S., Bell, A.M.T., Duller, G.A.T., Finch, A.A., Jain, M., King, G.E., Pearce, N.J., Roberts, H.M., 2021a. Exploring sources of variation in thermoluminescence emissions and anomalous fading in alkali feldspars. Radiat. Meas. 141, 106541.
Riedesel, S., Kumar, R., Duller, G.A.T., Roberts, H.M., Bell, A.M.T., Jain, M., 2021b. Site-selective characterisation of electron trapping centres in relation to chemistry, structural state and mineral phases present in single crystal alkali feldspars. J. Phys. Appl. Phys. 54 (38), 385107.
Sellwood, E.L., Guralnik, B., Kook, M., Prasad, A.K., Sohbati, R., Hippe, K., et al., 2019. Optical bleaching front in bedrock revealed by spatially-resolved infrared photoluminescence. Sci. Rep. 9 (1), 2611.
Sellwood, E., Kook, M., Jain, M., 2022. A 2D imaging system for mapping luminescence-depth profiles for rock surface dating. Radiat. Meas. 150, 106697.
Thomsen, K.J., Kook, M., Murray, A.S., Jain, M., 2018. Resolving luminescence in spatial and compositional domains. Radiat. Meas. 120, 260–266.
Thomsen, K.J., Murray, A.S., Jain, M., Bøtter-Jensen, L., 2008. Laboratory fading rates of various luminescence signals from feldspar-rich sediment extracts. Radiat. Meas. 43, 1474–1486.
Wintle, A.G., 1973. Anomalous fading of thermoluminescence in mineral samples. Nature 245, 143–144.